

P. C. Xia\*, K. Xie, H. Z. Cui and J. J. Yu

# Influence of Heat Treatment on $\gamma'$ Phase and Property of a Directionally Solidified Superalloy

DOI 10.1515/htmp-2016-0060

Received March 17, 2016; accepted January 13, 2017

**Abstract:** The effects of heat treatment process on microstructure and properties of a nickel base superalloy are investigated. The size of  $\gamma'$  phase decreases and the stress rupture life of alloy at 1100 °C/60 MPa drops with the rise of cooling rate. The hardness at room temperature also increases. The size of cuboidal  $\gamma'$  precipitate and the volume of spherical  $\gamma'$  precipitate increase with the rise of aging temperature. With higher aging temperature, the alloy exhibits bimodal  $\gamma'$  phase. A reasonable combination of the size and volume fraction of cuboidal and spherical  $\gamma'$  phase can obtain better stress rupture property at 1100 °C/60 MPa.

**Keywords:** nickel base superalloy, heat treatment,  $\gamma'$  phase, property

## Introduction

Superalloys have wide applications in aerospace and land-based gas-turbine engine [1–3]. In order to meet the severe environments, the alloys are required to possess the excellent properties such as high temperature strength, better oxidation and corrosion resistance, excellent fatigue and creep resistance, optimal stability of microstructure and service reliability, which can be achieved by solution and precipitation strengthening. Better mechanical properties can be attained by reasonable combination of the morphology, the size, the volume fraction and the distribution of strengthening phases [3, 4]. Xie et al. [5] investigated the influence of heat treatment regimes on microstructure and creep properties of FGH95 nickel base superalloy (FGH95

nickel base superalloy is manufactured via powder metallurgy processing routs). Results showed that coarser  $\gamma'$  precipitates of FGH95 nickel base superalloy were distributed in the previous particle boundaries (PPB) regions where was  $\gamma'$ -free after solid solution treatment. Fine  $\gamma'$  phase was dispersedly distributed in the grains, in addition, some (Nb, Ti)C particles precipitated along the boundaries, which was mainly responsible for better creep resistance and longer creep life in aerospace and land-based gas-turbine engine applications. It is well known that heat treatment has significant influence on morphology, size, volume fraction and distribution of the strengthening phase [6–10]. Van Sluytman et al. [11] investigated precipitate shapes in a series of new platinum group metal (PGM)-containing Ni-base alloys and concluded that a peak in the shape parameter ratio occurred when lattice misfit reaches some range. This peak was correlated with good high temperature mechanical properties, suggesting that precipitates had an “optimal” shape. Precipitates evolved to a stable “attractor” shape during short time aging under conditions where coherency was maintained. The mechanical properties of alloys will be greatly enhanced by reasonable heat treatment process [12–14]. The heat treatment includes solid solution treatment and aging treatment. The goal of solid solution treatment is to solute coarse precipitate and to reduce the volume fraction of  $\gamma + \gamma'$  eutectic. At the same time, it decreases the segregation of alloy elements. Aging treatment is conducted after solid solution treatment, which precipitates finer  $\gamma'$  phase and enhances the high temperature mechanical property of the alloy. Caron et al. [15] studied the effect of two heat treatments on the creep behavior of CMSX-2 superalloy in the temperature range of 760–1050 °C. The result showed that the heat treatment resulting in cuboidal precipitates with the size of 0.45  $\mu\text{m}$  led to a two-fold improvement in creep life over the corresponding values obtained with other heat treatment which produced smaller and more odd-shaped particles. Yu et al. [16] increase the creep rupture life of DD32 alloy by choosing a reasonable heat treatment. Therefore potential of an alloy can be further improved by choosing a reasonable heat treatment process. There are many papers on the

\*Corresponding author: P. C. Xia, School of Materials Science and Engineering, Shandong University of Science and Technology, Qingdao 266590, China, E-mail: xpc328@126.com

K. Xie, H. Z. Cui, School of Materials Science and Engineering, Shandong University of Science and Technology, Qingdao 266590, China

J. J. Yu, Institute of Metal Research, Chinese Academy of Sciences, Shenyang 110016, China

influences of cooling ways after solution treatment and temperature of high aging [17–19]. Masoumi et al. [20] investigated the reprecipitation mechanisms and kinetics of  $\gamma'$  particles during cooling from supersolvus and subsolvus temperatures in AD730TM Ni-based superalloy using Differential Thermal Analysis (DTA). A function for the kinetic parameter  $k(T)$  was developed and a new equation was proposed on the basis of experimental correlations between the cooling rate and the  $\gamma'$  precipitate size for continuous cooling from supersolvus temperatures. It is essential to investigate the effect of cooling ways after solid solution treatment and temperature of high aging on microstructure and property of the superalloy. It is of great significance to further improve the properties and excavate potential of experimental alloy.

## Experimental procedure

Experimental material has the compositions (wt.%): 0.05C, 9.0Cr, 5.0Co, 6.0Al, 3.0W, 3.0Mo, 2.2Nb, and bal. Ni. The alloy was first melted in a VZM-25F-type vacuum induction furnace. Then the directionally solidified samples with a diameter of 16 mm and length of 220 mm were made by HRS (high rate solidification) method in a ZGD2 type vacuum furnace with a temperature gradient of 60–80 °C/cm and a withdrawal rate of 6 mm/min. The solvus temperature of  $\gamma'$  phase is in the range of 1090 °C and 1190 °C. The effect of cooling ways after solution treatment on alloy was first studied. Solution temperature and holding time were the same at 1240 °C for 4 h, the alloy was then cooled respectively by air cooling (AC) and accessing air cooling (AAC). The average cooling rate of AC to AAC was about 22 °C/s and 31 °C/s respectively. Subsequently, the specimens were treated at 870 °C for 24 h and cooled freely in air. Secondly influence of aging temperature of high temperature properties of the alloy is studied. The alloy was first solution treated at 1240 °C for 4 h and cooled in air, then aging treatment was done. Aging treatment included high temperature and low temperature aging treatments. Aging temperatures of high temperature were separately 1100 °C, 1130 °C, 1150 °C for 4 h followed by cooled in air. Finally the specimens were treated at 870 °C for 24 h and cooled in air. The stress rupture specimens having a 5 mm gauge diameter and a 25 mm gauge length were machined by precision grinding from heat-treated specimens. F-25 type stress rupture testing machine was used to test the stress rupture properties of alloys at 1100 °C/60MPa. The stress rupture life and elongation were the average values of three data.

Hardness was examined at room temperature by HB-3000 Brinell hardness tester with the load of 9807N and the loading time of 20s. Five points were tested every specimen. Each data point represents an average of 15 readings (three specimens).

Scanning electron microscope (SEM) and transmission electron microscope (TEM) were used to observe microstructures of alloy. The SEM specimens were electrolyzed in a solution of 20 ml  $\text{HNO}_3$  + 40 ml  $\text{CH}_3\text{COOH}$  + 340 ml  $\text{H}_2\text{O}$  at a voltage of 7 volt. JSM-E001F SEM with a cold field emission gun was used to examine the  $\gamma'$  phase. The TEM specimens with the thickness of 600nm were cut by through the wire cutting machine about 5 mm far away the stress rupture fracture. The specimens were finally thinned by double-jet electrolyte machine in a solution of 30 ml  $\text{HClO}_4$  + 270 ml  $\text{CH}_3\text{CH}_2\text{OH}$  at –30 °C. The dislocation configuration was observed by using Philip EM420 TEM.

Five SEM pictures of  $\gamma'$  phase in the dendrite and five SEM pictures of  $\gamma'$  phase in the interdendrite are randomly chosen to decide the volume fraction of  $\gamma'$  precipitate. Every size of  $\gamma'$  phase is measured in each picture. Then the total area of  $\gamma'$  phase is calculated. The percent of  $\gamma'$  phase in every picture is determined. The volume fraction of  $\gamma'$  precipitate is the average value of ten pictures.

## Results

### Influence of cooling ways after solid solution treatment

Table 1 shows the 1100 °C/60MPa stress rupture properties of alloy cooled by AC and AAC. It demonstrates that stress rupture properties of alloys after heat treatment are superior to that of the as-cast alloy. The stress life of the alloy cooled by AC is the longest. It is accordant with the experimental results of Van Sluytman et al. [11]. According to the computational formula of shape parameter  $\eta$  [11],  $\eta$  of  $\gamma'$  precipitates are respectively 0.13 and 0.07 corresponding to the alloy cooled by AC and AAC, respectively. The alloy cooled by AC has better high

**Table 1:** The stress rupture property of alloy at 1100 °C/60MPa and HB of alloy at room temperature by different cooling ways.

Stress rupture property	As-cast alloy	Alloy by AC	Alloy by AAC
Stress rupture life (h)	57.9	78.0	65.5
Elongation ( % )	24.2	26.8	36.4
Hardness (HB)	324	378	405

temperature stress rupture property. The change of room hardness is different from that of stress life. The alloy cooled by AAC has the highest hardness (Table 1).

The morphology of  $\gamma'$  phase of the alloys with different cooling ways is shown in Figure 1. The  $\gamma'$  phase of as-cast alloy is irregular cubical (Figure 1(a)). The size of  $\gamma'$  precipitate is about 380 nm and the volume fraction is about 58%. The size of  $\gamma'$  phase decreases and the morphology of  $\gamma'$  phase changes from cuboid (Figure 1(a)) to sphere (Figure 1(b) and (c)) during heat treatment. The sizes of  $\gamma'$  phases are about 200 nm (diameter of sphere) and 130 nm (diameter of sphere) according to AC and AAC.

## Influence of aging temperature

The stress rupture property of alloy after different aging treatments at 1100 °C/60MPa is shown in Table 2. It reveals that the change of stress rupture life is minor from 1100 °C to 1130 °C, the stress rupture life increases at 1150 °C. The trend of elongation change is reverse to the stress rupture life. The hardness modification at room temperature is similar to that of stress rupture life (Table 2). The alloy aged at 1150 °C has the highest hardness.

Figure 2 shows the morphology of  $\gamma'$  precipitates with various aging treatments. It demonstrates that the size of cubic  $\gamma'$  phase rises with increasing aging temperature. The spherical  $\gamma'$  phase is precipitated gradually. The higher the aging temperatures, the larger the size of cubic  $\gamma'$  phase and the more the volume fraction of  $\gamma'$  in spherical shape (Figure 2(c)).

## Discussion

### Influence of cooling ways on $\gamma'$ phase and property of alloy

The morphology and size of  $\gamma'$  phase are related to the cooling rate after solid solution treatment. There is no

**Table 2:** The stress property of alloy at 1100 °C/60MPa and HB of alloy at room temperature by different aging temperatures.

Stress rupture property	1100 °C	1130 °C	1150 °C
Stress rupture life (h)	78.6	90.8	104.7
Elongation ( % )	39.3	48.5	59.2
Hardness (HB)	302	338	382

bigger  $\gamma'$  phase in Figure 1(b) and (c), which indicates that coarse  $\gamma'$  phase of as-cast alloy has completely dissolved when alloy is solid soluted at 1240 °C. The cooling rate is fast for AAC, thereby it is easy to nucleate and the number of nucleation sites increases. When the surface energy predominates, the surface area of sphere is minimum under the condition of constant volume, so  $\gamma'$  phase is spherical and has small size. The quicker the cooling rate is, the smaller the size of the particles is (Figure 1(b) and (c)). However the fraction of  $\gamma'$  volume through different ways remains unchangeable (about 62%).

The stress rupture properties of nickel base superalloy with different cooling ways are mainly dependent on the morphology, size, volume fraction and distribution of  $\gamma'$  strengthening phase. The size of  $\gamma'$  precipitate changes with different cooled ways. The  $\gamma'$  size by AC is large and the rupture life at 1100 °C/60MPa is long. The alloy cooled by AAC has small  $\gamma'$  phase and short stress rupture life. The dislocations reinforce alloy by shearing  $\gamma'$  precipitates at high temperature and low stress (Figure 3). Figure 3(a) shows the dislocation configuration of alloy cooled by AC after stress rupture fracture at 1100/60MPa. It demonstrates that many dislocations or dislocation pairs (Figure 3(a) arrow indicated) shear the  $\gamma'$  precipitates. The dislocations in matrix start to move in the action of stress at the first stage of stress deformation. They are blocked by  $\gamma'$  phase and begin to shear  $\gamma'$  precipitate for the low strength of  $\gamma'$  precipitates at high temperature. The stress-induced deformation increases with the rise of dislocation shearing  $\gamma'$  precipitate. The  $\gamma'$  precipitates coarsen and raft at the last stage of deformation. There are many dislocations in

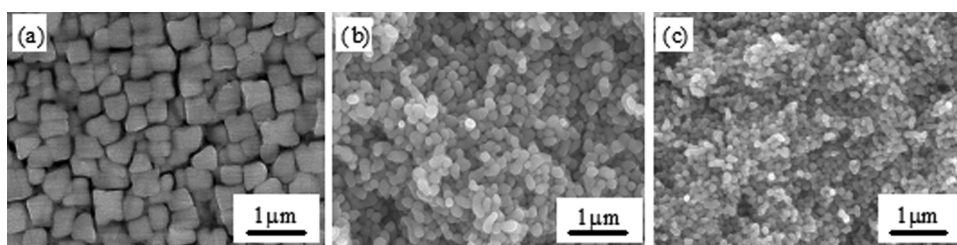


**Figure 1:** The morphology of  $\gamma'$  phase of alloy by different cooling ways (a) as-cast alloy, (b) alloy cooled by AC, (c) alloy cooled by AAC.

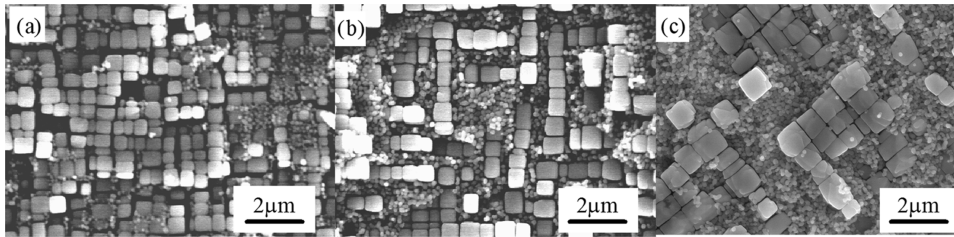


**Figure 2:** Influence of aging temperature of elevate temperature on  $\gamma'$  precipitate (a) 1100 °C, (b) 1130 °C, (c) 1150 °C.

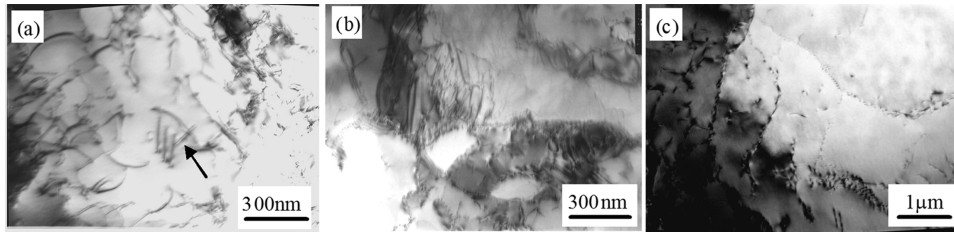


**Figure 3:** Dislocation configuration of alloy by different cooling ways after stress rupture fracture at 1100 °C /60MPa (a) dislocations and dislocation pairs shearing  $\gamma'$  precipitate for the alloy by AC (b) high density dislocation around  $\gamma'$  rafting for the alloy cooled by AC (c) dislocations in and around  $\gamma'$  rafting for the alloy cooled by AAC.

the  $\gamma'$  rafts (Figure 3(a)). High-density dislocations assemble around  $\gamma'$  rafting (Figure 3(b)), which offers better strength for the alloy. The experimental results of Han et al. demonstrated also that dislocation networks were formed at  $\gamma/\gamma'$  interfaces and the  $\gamma'$  rafts were sheared by dislocation pairs during creep test at 1040 °C [21]. The deformation structure of the alloy cooled by AAC is the same as that by AC. The dislocation strengthens alloy by the shearing  $\gamma'$  phase (Figure 3(c)).  $\gamma'$  precipitates raft at the course of stress rupture test. There are lots of dislocations in and around the  $\gamma'$  rafting. The strengthening way by AC and AAC is the same. The dislocations reinforce the alloy by shearing  $\gamma'$  phase when the size of  $\gamma'$  phase is not large enough according to the strengthening mechanism. The shearing stress rises with the increase of  $\gamma'$  size. Therefore the strengthening effect is better and the stress rupture life of alloy by AC is longer. It is easy for dislocation to shear  $\gamma'$  phase of AAC alloy for small  $\gamma'$  size. So it has large deformation before stress rupture fracture. The alloy by AAC has longer elongation. In fact the grain boundary has certain effect on the stress rupture life. There are many carbides in the grain boundary and interdendrite [22]. The expand coefficient is different between matrix and carbide with the increase of temperature during stress rupture experiment, which results in large stress in the interface. The higher the temperature, the larger the stress. It will produce crack in the interface when the stress exceeds the bond strength between matrix and carbide at high temperature. So it is easy for the cracks to initiate by carbide and propagate along grain

boundary. If the carbides have the shape long strip and continuously distribute in the grain boundary, the superalloy has short stress rupture life. The carbides change little block and the distribution is discontinuous in grain boundary by heat treatment. It is difficult for crack to initiate and propagate in the grain boundary. The stress rupture life of alloy is long [22]. The change at room temperature hardness is converse to the stress rupture life. The alloy by AAC has high room temperature hardness, which is contributed to dislocation strengthening. It is difficult for dislocations to shear  $\gamma'$  precipitate for high strength at room temperature. The  $\gamma'$  size is small and the distance between  $\gamma'$  precipitates is short for the alloy by AAC. The effect of strengthening at room temperature is superior to that of alloy by AC. The alloy by AAC has high room temperature hardness.

## Influence of aging temperature on $\gamma'$ phase and property

There are  $\gamma'$  precipitates with various shape and size, which indicates that the aging temperature is between first solution temperature and fully solution temperature of  $\gamma'$  phase. The  $\gamma'$  precipitates dissolve into matrix and the alloy repeatedly precipitates fine and spherical  $\gamma'$  phase during the following cooling. The higher the aging temperature, the more volume fraction of  $\gamma'$  solution. The volume fraction of cubical  $\gamma'$  precipitate reduces with the rising temperature of aging treatment. Spherical  $\gamma'$  phase is precipitated from the supersaturated solution

during aging treatment. The diffusion rate of element is quick at high temperature, which is advantageous for  $\gamma'$  phase to grow. Thereby the growing rate of  $\gamma'$  phase is faster and the size of cubic  $\gamma'$  phase is larger at higher aging temperature (Figure 2(c)).

The stress rupture property of alloy with different aging treatments at 1100 °C/60MPa depends on the shape, the size, and the fraction volume of  $\gamma'$  phase. Figure 4 shows the dislocation structure at aging temperature of 1130 °C. There are many dislocations trapped within the  $\gamma'$  precipitates and lots of dislocations assemble around  $\gamma'$  phase (Figure 4(a)).  $\gamma'$  phase coarsens and makes irregular long strips at the last stage of stress rupture. There are high density of dislocations around  $\gamma'$  phase (Figure 4(b)). It is difficult for dislocations to shear or bypass the large  $\gamma'$  phase. The dislocations have to assemble the around  $\gamma'$  phase or climb over  $\gamma'$  phase [23]. The size of cubical  $\gamma'$  precipitate and the volume fraction of spherical  $\gamma'$  phase is small when the alloy is aged at 1100 and 1130 °C. Thereby the stress rupture life is similar. The cubical  $\gamma'$  size and the volume fraction of spherical  $\gamma'$  precipitate greatly increase when the alloy is aged at 1150 °C (Figure 2(c)). The large  $\gamma'$  phase has better strengthening effect in alloy. The stress rupture life of alloy with aging temperature of 1150 °C is longest. The size of cubical  $\gamma'$  phase rises with increasing aging temperature and the distance between cubical  $\gamma'$  phase is broad. The dislocations can slide without block in the matrix during stress rupture test. Thereby the elongation increases with the rising aging temperature. The change tendency of hardness at room temperature is similar to stress rupture life. The large volume fraction of fine and spherical  $\gamma'$  precipitates is contributed to the high hardness at room temperature when aged at 1150 °C.

It is worth noting that the creep temperature (1100 °C) is higher than the initial solution temperature of  $\gamma'$  phase (1090 °C). The spherical  $\gamma'$  precipitates can dissolve into matrix. But the temperature difference is small. It takes

some time for little  $\gamma'$  precipitates to dissolve into matrix in the course of stress rupture test. Many elements such as Cr, Mo, W, Co and Nb solute into  $\gamma'$  phase, which improves the stability and solvus temperature of  $\gamma'$  phase. The volume fraction of  $\gamma'$  precipitates dissolves into matrix is small during stress rupture test. Most of  $\gamma'$  precipitates start to grow and coarse. The  $\gamma'$  phase finally form irregular long strip (Figures 3 and 4). The more the volume fraction of  $\gamma'$  precipitates, the longer the time of dissolving into matrix. The alloy is strengthened through dislocation shearing spherical  $\gamma'$  precipitates at the beginning stage of creep. The cubical  $\gamma'$  phase grows with the dissolving into matrix of spherical  $\gamma'$  precipitate in the course of stress rupture test. It is more difficult for dislocation to bypass the large  $\gamma'$  phase. The alloy with aging temperature of 1150 °C has the longest life of stress rupture. The room hardness mainly depends on the size and distribution of fine and spherical  $\gamma'$  precipitates. The dislocations strengthen alloy by shearing spherical  $\gamma'$  precipitates. The smaller the size of  $\gamma'$  precipitate, the larger volume fraction of  $\gamma'$  precipitate, the higher the hardness at room temperature.

## Conclusions

- 1) The size of  $\gamma'$  phase decreases and the stress rupture life of alloy at 1100 °C/60MPa drops with the rise of cooling rate. However, the hardness of room temperature increases.
- 2) The size of cuboidal  $\gamma'$  phase and the volume of spherical  $\gamma'$  phase increase with the rise in the aging temperature. Bimodal  $\gamma'$  phase is achieved at higher aging temperature. The stress rupture life at 1100 °C /60MPa and room temperature hardness rises with increasing aging temperature.
- 3) Better stress rupture property at 1100 °C/60MPa may be obtained by reasonable combination of the size

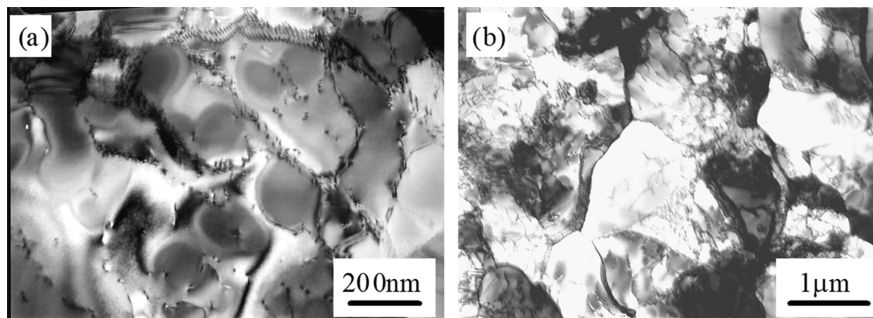


**Figure 4:** Dislocation configuration of alloy at the aging temperature of 1130 °C after stress rupture fracture at 1100 °C /60MPa (a) dislocations shearing  $\gamma'$  precipitate (b) high density dislocation around  $\gamma'$  phase.

and volume fraction of cuboidal and spherical  $\gamma'$  phase. The smaller the size of  $\gamma'$  precipitate, the larger volume fraction of  $\gamma'$  precipitate, the higher the hardness at room temperature.

**Funding:** This work was financially supported by the National High Technology Research and Development Program of China (863 Program) (SS2015AA031901), Taishan Scholars Project of Shandong (ts20110828), National Natural Science Foundation of China (51272141, 51208288). The authors are grateful for those supports.

## References

1. Sims CT, Stoloff NS, Hagel WC. *Superalloys II*. New York: John Wiley & Sons, 1987.
2. Matthew J, Donachie J. *Superalloy*. Metal Park, OH: American Society for Metals, 1984.
3. Pollock TM, Tin S. Nickel-based superalloys for advanced turbine engines: chemistry, microstructure, and properties, *J Prop Power* 2006;22:361–374.
4. Mughrabi H. Microstructural aspects of high temperature deformation of monocrystalline nickel base superalloys: some open problems, *Mater Sci Technol* 2009;25:191–204.
5. Xie J, Tian SG, Zhou XM, Yu XF, Wang WX. Influence of heat treatment regimes on microstructure and creep properties of FGH95 nickel base superalloy, *Mater Sci Eng* 2012; A538:306–314.
6. Safari J, Nategh S. On the heat treatment of Rene-80 nickel-base superalloy, *J Mater Process Technol* 2006;176:240–250.
7. Monajati H, Jahazi M, Bahrama R, Yue S. The influence of heat treatment conditions on  $\gamma'$  characteristics in Udimet 720, *Mater Sci Eng* 2004;A373:286–293.
8. Fuchs GE. Solution heat treatment response of a third generation single crystal Ni-base superalloy, *Mater Sci Eng* 2001; A300:52–60.
9. Miller MK, Babu SS, Vitek JM. Stability of  $\gamma'$  precipitates in a PWA1480 alloy, *Intermetal* 2007;15:757–766.
10. John HS, Ramon A, Jose LM. Thermal characterization of a Ni-based superalloy, *Thermoch Acta* 2002;392–393:295–298.
11. Van Sluytman JS, Pollock TM. Optimal precipitate shapes in nickel-base  $\gamma$ - $\gamma'$  alloys, *Acta Mater* 2012;60:1771–1783.
12. He LZ, Zheng Q, Sun XF, Guan HR, Hu ZQ. Effect of heat treatment on microstructures and tensile properties of Ni-base superalloy M963, *Mater Sci Eng* 2005;A398:128–136.
13. Li P, Li S, Han YF. Influence of solution heat treatment on microstructure and stress rupture properties of a  $\text{Ni}_3\text{Al}$  base single crystal superalloy IC6SX, *Intermetallic* 2011;19:182–186.
14. Mehdi R, Srdjan M, Ilchat S. Microstructure and hardness evolution in MAR-M247 Ni-based superalloy processed by controlled cooling and double heat treatment, *J Alloy Com* 2013;550:339–344.
15. Caron P, Khan T. Improvement of creep strength in a nickel-base single-crystal superalloy by heat treatment, *Mater Sci Eng* 1983;61:173–184.
16. Yu JJ, Sun XF, Zhao NR, Jin T, Guan HR, Hu ZQ. Effect of heat treatment on microstructure and stress rupture life of DD32 single crystal Ni-base superalloy, *Mater Sci Eng* 2007;A460–A461:420–427.
17. Singh ARP, Nag S, Hwang JY, Viswanathan GB, Tiley J, Srinivasan R, et al. Influence of cooling rate on the development of multiple generations of  $\gamma'$  precipitates in a commercial nickel base superalloy, *Mater Charact* 2011;62:878–886.
18. Radis R, Schaffer M, Albu M, Kothleitner G, Pöhl P, Kozeschnik E. Multimodal size distributions of  $\gamma'$  precipitates during continuous cooling of UDIMET 720 Li, *Acta Mater* 2009;57:5739–5747.
19. Singh ARP, Nag S, Chattopadhyay S, Ren Y, Tiley J, Viswanathan GB, et al. Mechanisms related to different generations of  $\gamma'$  precipitation during continuous cooling of a nickel base superalloy, *Acta Mater* 2013;61:280–293.
20. Masoumi F, Shahriari D, Jahazi M, Cormier J, Devaux A. Coarsening and dissolution of  $\gamma'$  precipitates during solution treatment of AD730<sup>TM</sup> Ni-based superalloy: Mechanisms and kinetics models, *J Alloy Com* 2016;658:981–995.
21. Han GM, Yu JJ, Hu ZQ, Sun XF. Creep property and microstructure evolution of a nickel-base single crystal superalloy in [011] orientation, *Mater Charact* 2013;86:177–184.
22. Xia PC, Yu JJ, Sun XF, Guan HR, Hu ZQ. Influence of heat treatment on the microstructure and stress rupture property of DZ951 alloy, *J Mater Process Technol* 2007;186:315–322.
23. Hafez Haghighat SM, Eggeler G, Raabe D. Effect of climb on dislocation mechanisms and creep rates in  $\gamma'$ -strengthened Ni base superalloy single crystals: A discrete dislocation dynamics study, *Acta Mater* 2013;61:3709–3723.